ADVANCED MATERIALS

www.advmat.de

Electrically Controllable Molecularization of Terahertz Meta-Atoms

Hyunseung Jung, Jaemok Koo, Eunah Heo, Boeun Cho, Chihun In, Wonwoo Lee, Hyunwoo Jo, Jeong Ho Cho, Hyunyong Choi, Moon Sung Kang, and Hojin Lee**

Active control of metamaterial properties is critical for advanced terahertz (THz) applications. However, the tunability of THz properties, such as the resonance frequency and phase of the wave, remains challenging. Here, a new device design is provided for extensively tuning the resonance properties of THz metamaterials. Unlike previous approaches, the design is intended to control the electrical interconnections between the metallic unit structures of metamaterials. This strategy is referred to as the molecularization of the meta-atoms and is accomplished by placing graphene bridges between the metallic unit structures whose conductivity is modulated by an electrolyte gating. Because of the scalable nature of the molecularization, the resonance frequency of the terahertz metamaterials can be tuned as a function of the number of meta-atoms constituting a unit metamolecule. At the same time, the voltage-controlled molecularization allows delicate control over the phase shift of the transmitted THz, without changing the high transmission of the materials significantly.

Arrays of metallic structures with micrometer-scale periodicity can resonate with incident terahertz (THz) waves. Emphasizing the unique properties that are not achievable in nature, such structures are called THz metamaterials.[1] THz metamaterials open unprecedented opportunities in the fields of next-generation communication,[2,3] sensing,[4,5] and imaging systems.[6,7] To fully exploit the THz metamaterials, actively driven device platforms that can modulate their optical response by external control are highly desirable; the resonance frequency and phase of the incident wave, as well as its transmission, reflectance, and absorbance, should be tuned widely and accurately. Although various tuning methods based on executing optical,[8–10] electrical,[11–13] thermal,[14,15] or mechanical[16–18] means have been developed, these strategies try to alter the electromagnetic properties of either the surrounding environment of the enclosed metamaterials, or to control the physical properties of unit structures of metamaterials (often referred to as meta-atoms).[19–21] While such strategies have successfully demonstrated extensive modulation in the transmission of THz metamaterials at their given resonance frequency, active control of the resonance frequency is hardly achievable, because the fundamental resonance frequency of a metamaterial is dominantly governed by the characteristics of the structures and their arrangements, with only a limited margin for modulation at varied surrounding conditions. Alternative strategies of directly manipulating the meta-atoms may circumvent this issue. However, the largest variation experimentally attained so far has reached about 30% of the fundamental resonance frequency.[19] Moreover, because designing an electrical driving scheme that does not interfere with the THz response of the metamaterials is another challenging issue, most active devices reported so far have adopted bulky optical pumping methods. A few experimental reports on electrically driven active THz metamaterials incorporated with electrical lines have only shown the switching characteristics of the resonance, but they could not tune the frequency of the resonance.[22,23]

To overcome the above issues, a completely different aspect in designing devices may be necessary for developing electrically driven active THz metamaterials. Instead of modulating the individual properties of the unit metastructures, controlling the connectivity between meta-atoms can provide versatile opportunities. We refer to this new concept as the molecularization of meta-atoms, which can control the electrical connection between meta-atoms. By changing the physical

H. Jung, E. Heo, Prof. H. Lee
School of Electronic Engineering
Soongsil University
Seoul 06978, South Korea
E-mail: hojinl@ssu.ac.kr

J. Koo, B. Cho, H. Jo, Prof. M. S. Kang
Department of Chemical Engineering
Soongsil University
Seoul 06978, South Korea
E-mail: mskang@ssu.ac.kr

C. In, Prof. H. Choi
School of Electrical and Electronic Engineering
Yonsei University
Seoul 03722, South Korea

W. Lee, Prof. H. Lee
Department of Information Communication, Materials, and Chemistry Convergence Technology
Soongsil University
Seoul 06978, South Korea

Prof. J. H. Cho
School of Chemical Engineering
SKKU Advanced Institute of Nanotechnology (SAINT)
Sungkyunkwan University
Suwon 16419, South Korea

DOI: 10.1002/adma.201802760

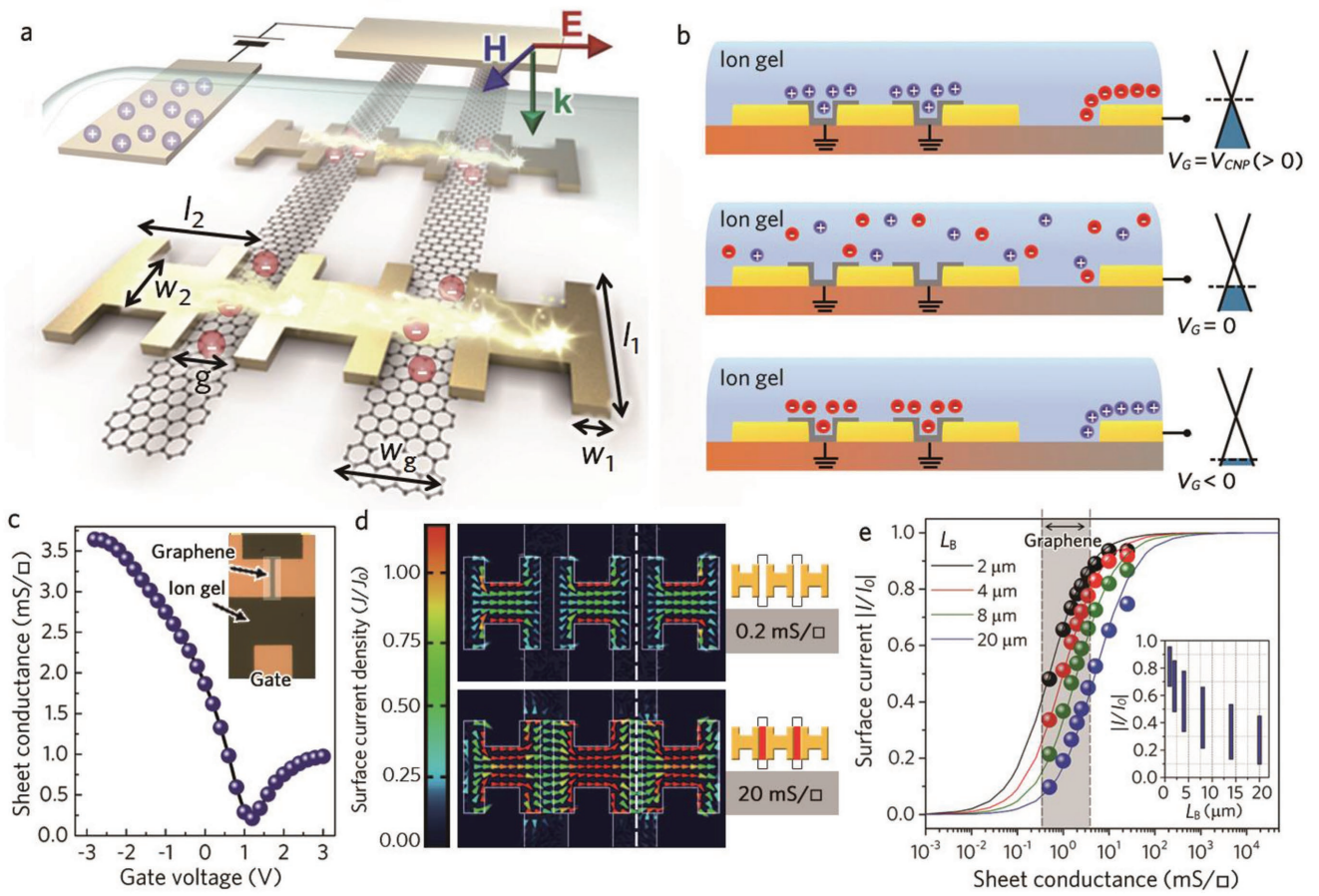

Figure 1. Electrically controllable molecularization of H-shaped meta-atoms. a) Schematic image of the proposed metamaterials. w_1 = 10 μm, w_2 = 20 μm, l_1 = 50 μm, l_2 = 40 μm, g = 8 μm, and w_g = 22 μm. b) Schematic of controlling the conductivity of graphene bridges in contact with an ion-gel electrolyte by applying voltages to gate (V_G). c) Sheet conductance of a graphene bridge at different gate-bias conditions. d) Normalized surface-current density of metamolecules containing bridges with different sheet conductances. The surface current is calculated by the line integral of the surface-current density, indicated by the dashed line. e) Summary of the degree of molecularization for metamolecules (M) containing bridges with different lengths (L_B) and different sheet conductances. The inset summarizes the accessible range of M for metamolecules containing graphene bridges of different lengths.

dimensions of the repeating units of metamaterials through the molecularization of meta-atoms, active control of the THz response can be achieved. This strategy is expected to greatly enlarge the range of THz modulation, since the control is not designed to induce a relatively minute influence within the meta-atoms, but is intended to introduce a variation between the meta-atoms which, in principle, can be extended over the entire metamaterial.

We demonstrate electrically controlled molecularization of THz meta-atoms by means of a system consisting of the following three critical components: i) arrays of metallic meta-atoms, ii) graphene bridges that connect the meta-atoms, and iii) an electrolyte-gating system that modulates the conductivity of the graphene bridges. By forming metamolecules from discrete meta-atoms, we can tune the THz resonance frequency as a function of the number of meta-atoms in a unit metamolecule. Theoretically, this can be extended to yield nearly infinite modulation ratio (= the fundamental frequency of the meta-atoms/the fundamental frequency of the metamolecule). The strategy also allows precise and wide control of the phase of the transmitted THz wave at a designated frequency as a function of applied voltage, while preserving the transmittance. Moreover, we emphasize that the highly tunable metamateirals could be prepared in a simple device configuration that does not require complicated operating methods and fabrication processes.

Figure 1a shows the structure of our active THz metamaterial system. Arrays of H-shaped gold meta-atoms serve as the building blocks of the metamaterials, which exhibit specific resonances with the incident THz wave. Patterned graphene bridges form electrical connections between the meta-atoms. A layer of electrolyte is placed on top of the gold arrays and graphene bridges. The layer enables the conductivity of the graphene bridges to be modulated by means of electrochemical capacitive coupling.[24–27] A solid-state ion gel consisting of ionic liquid confined in a block copolymer matrix is employed for the electrolyte. Because of the electric-double layer formation, electrolyte-gating system can still operate even when the gate electrode is not placed on top of the graphene, but is completely offset from the graphene channel (Figure 1b).[26] Being

able to modulate the conductivity of graphene from an offset gate is critical for allowing the incident THz wave to interact only with the arrays of meta-atoms, but not with the metallic gate electrodes. Figure 1c shows the above modulation characteristics of graphene-sheet conductance (σ_s) attained from an electrolyte-gated graphene transistor with the offset gate having a channel dimension equivalent to that of the graphene bridges for our metamaterials.

We have confirmed our device concept by performing full-wave 3D electromagnetic simulations; the operation of the molecularization system could be explained using the normalized surface-current density distribution of the H-shaped gold meta-atoms connected by bridges with different values of σ_s (Figure 1d). For the simulation, the length (L_B) and width (W_B) of the bridge between the meta-atoms were set to 8 and 50 μm, respectively. For bridges with a low sheet conductance (σ_s = 0.2 mS $\square^{-1}$, upper panel), the induced surface current was confined to the H-shaped meta-atoms, whereas for those with a high sheet conductance (σ_s = 20 mS $\square^{-1}$, lower panel), the neighboring atoms were electrically connected. These results support that the success of the active molecularization of meta-atoms hinges on controlling the conductance of the bridge.

For quantitative analysis, the degree of molecularization of the metamaterials (M) is parameterized as the normalized surface current of the bridges (I) divided by the surface current of the metallic metamolecules (I_0); I and I_0 could be obtained from the line integral of surface-current density across the graphene bridge and the metallic bridge, respectively (dashed line in Figure 1d). M = 0 corresponds to the case of fully isolated meta-atoms, which we term the fully atomized state of the metamaterial. On the other hand, M = 1 represents fully connected meta-atoms, which we term the fully molecularized state of the metamaterial. The green circles in Figure 1e plot M as a function of the sheet conductance of the bridge layer. The data can be reproduced very well using the following formula

$$M = \frac{I}{I_0} = \frac{\sigma_s}{G_M(L_B/W_B) + \sigma_s} \quad (1)$$

where G_M is the reference conductance yielding M = 0.5, and equals 12.5 mS in our structures. The plot clearly shows that a dramatic change in M occurs within a limited range of σ_s; M changes from 0.1 to 0.9 as σ_s varies by less than two orders of magnitude. Thus, to execute the active molecularization of meta-atoms effectively, finding an optimal bridging material that yields the conductance (= $\sigma_s \cdot W_B/L_B$) near G_M is critical. Figure 1c shows that at its charge neutral-point voltage (V_{CNP} = 1 V), the lowest σ_s of graphene is 0.3 mS $\square^{-1}$; and when V_G = −3 V, it can be increased up to 3.6 mS $\square^{-1}$. Even though the sheet conductance of graphene could be controlled only by an order of magnitude,[27,28] using graphene as the bridging material could still yield fairly good control over the molecularization of metamaterials (the achievable range of sheet conductance is shaded in grey in Figure 1e).

We also carried out additional analysis to optimize the device geometry. Varying L_B can have a meaningful impact on the modulation range of M, since the bridge geometry also determines its conductance (see details in Figure S5, Supporting Information). The inset in Figure 1e summarizes the modulation range of M for meta-atoms separated with various L_Bs, which was obtained by numerical analysis over different values of σ_s for graphene bridges (0.3–3.6 mS $\square^{-1}$). When L_B is as small as 2 μm, the variation of M at a given range of σ_s lies closer to 1. This indicates that the meta-atoms are barely isolated even when graphene bridges are at their low conductance states. On the other hand, when L_B is as large as 20 μm, the variation of M lies closer to 0. This implies that the electrical connection between meta-atoms would not be strong enough even when graphene bridges are at their high conductance states. The geometry of gold meta-atoms for the maximal modulation range of M was found to be 8 μm, and this geometry was employed to fabricate our active THz metamaterials system.

Figure 2a shows a series of optical microscope images of different-sized metamolecules. Following our prediction described above, we constructed metamolecules of different sizes by placing the graphene bridges with different periodicities. For the metamolecules in the first column, the graphene bridges were placed at every other gap between the meta-atoms. When all graphene bridges were in their conductive state, they formed dimeric metamolecules. By extending this approach, we also created larger metamolecules, such as trimeric metamolecules (the second column), and tetrameric metamolecules (the third column). Figure 2b shows the electric field distributions in metamolecules at different states of molecularization that are obtained by assuming different values of σ_s for the bridges. The upper panels are when σ_s = 0.3 mS $\square^{-1}$ is assumed, which matches with the lowest sheet-conductance value of our graphene attained at $V_G = V_{CNP}$ = 1 V. The results show the presence of a resistive potential barrier between meta-atoms preventing the formation of interatomic conducting paths. Meanwhile, the lower panels are when σ_s = 3.6 mS $\square^{-1}$ is assumed, which corresponds to the largest sheet conductance achievable at V_G = −3 V. One key demonstration is that by controlling the potential barrier between the bridge and meta-atom interface, meta-atoms can be conductively connected to extend their induced current path along the molecules of any size.

Figure 2c,d shows the simulated and experimental THz transmission spectrum for these metamolecules at different σ_s values and corresponding V_Gs, respectively. Because our molecularization system is remarkably simple and shows good mechanical endurance for bending (Figure S1, Supporting Information), the proposed samples can be easily fabricated on a highly flexible and THz-transparent polyimide substrate. Accordingly, the simulation and experimental transmission spectra show the absolute values against the air reference, not the modified values normalized by the underlying substrates. By applying V_G between +1 and −3 V, the transmission spectrum could be modulated gradually between the two V_G ends. The dimeric metamolecules displayed a redshift in the resonance frequency of as large as 0.30 THz from the fundamental resonance frequency of the given meta-atom array, i.e., 1.30 THz. For the trimeric and tetrameric metamolecules, this shift could be increased up to 0.52 THz and 0.67 THz, respectively. These values are larger than the shifts in any previous report on active THz metamaterials, which highlights the impact of our approach.

The molecularization of meta-atoms also provides a versatile platform to control the transmission (T) of THz waves at a

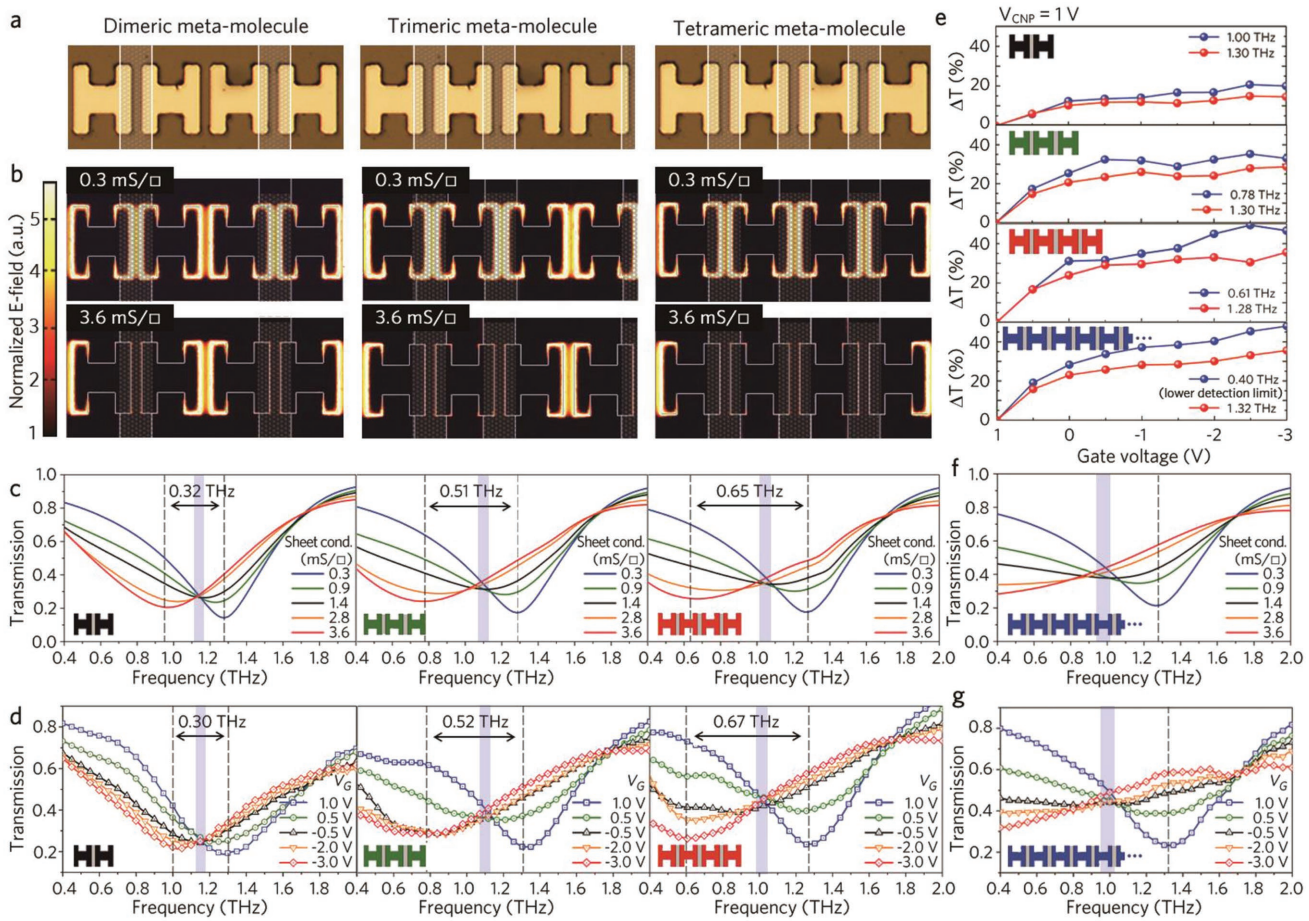

Figure 2. Transmission of different-sized metamolecules (simulation and experimental results). a) Optical microscopy images of the dimeric, trimeric, and tetrameric metamolecules. The graphene bridges are demarcated by white lines for the clarity. b) Normalized electric field distribution of the corresponding metamolecules at V_G = 1.0 V (V_{CNP}) (upper panel) and V_G = −3.0 V (lower panel), respectively. c) Simulated and d) experimental transmission spectra of the metamolecules at different sheet conductances of the bridges and corresponding gate voltages, respectively. e) Summary of the simulated transmission difference of dimeric, trimeric, tetrameric, and polymeric metamolecules at the fundamental resonance frequencies of their atomized state (red) and molecularized state (blue). f) Simulated and g) experimental transmission spectra of the polymeric metamolecules at different sheet conductances of the bridges and corresponding gate voltages, respectively.

designated frequency. Figure 2e summarizes the gate-tunable transmission of the metamaterials obtained at two fixed THz frequencies corresponding to the resonance frequency in the atomized state (V_G = +1 V, red) and that in molecularized state (V_G = −3 V, blue). We emphasize that the values are the absolute difference in transmission (ΔT), instead of the normalized transmission modulation depth.[14] As V_G changed from +1 to −3 V, the ΔT values for all the different-sized metamolecules were larger than 20%. The value for the tetrameric metamolecules was as high as 49.3% at 0.61 THz, which is the largest absolute ΔT obtained experimentally from the state-of-the-art THz modulators.[23] The summary plot also includes the results from polymeric metamolecules (Figure 2f,g), in which every gap between the meta-atoms in the array is entirely connected with graphene bridges. The polymeric metamolecules yielded a large ΔT of 47.9% at the lower limit of our measurement system (0.40 THz), which could be even larger at lower frequencies. The results above demonstrate the scalability of our molecularization systems for producing a THz switching device. Moreover, we confirmed that the switching behavior was reproducible over repeated cycles of molecularizing and atomizing the metamaterials (see details in Figure S7, Supporting Information).

Additionally, the molecularization of meta-atoms could largely control the phase of the incident THz wave, without changing the absolute transmission of the system. This is a very significant achievement for constructing active metasurfaces such as multifocus flat metalenses or beam steering applications. The phase of the transmitted wave is proportional to the derivative of the transmitted amplitude of the metamaterials with respect to the frequency.[29] Therefore, considerable phase changes ($\Delta\phi$) at a given frequency can be expected when the slope of the transmission spectra changes drastically between the atomized and molecularized states of the metamolecules. Interestingly, there is a very narrow frequency zone where the transmission curves of the atomized and molecularized resonances overlap (blue shade in Figure 2c,f). While the change of the transmission at different states of molecularization is

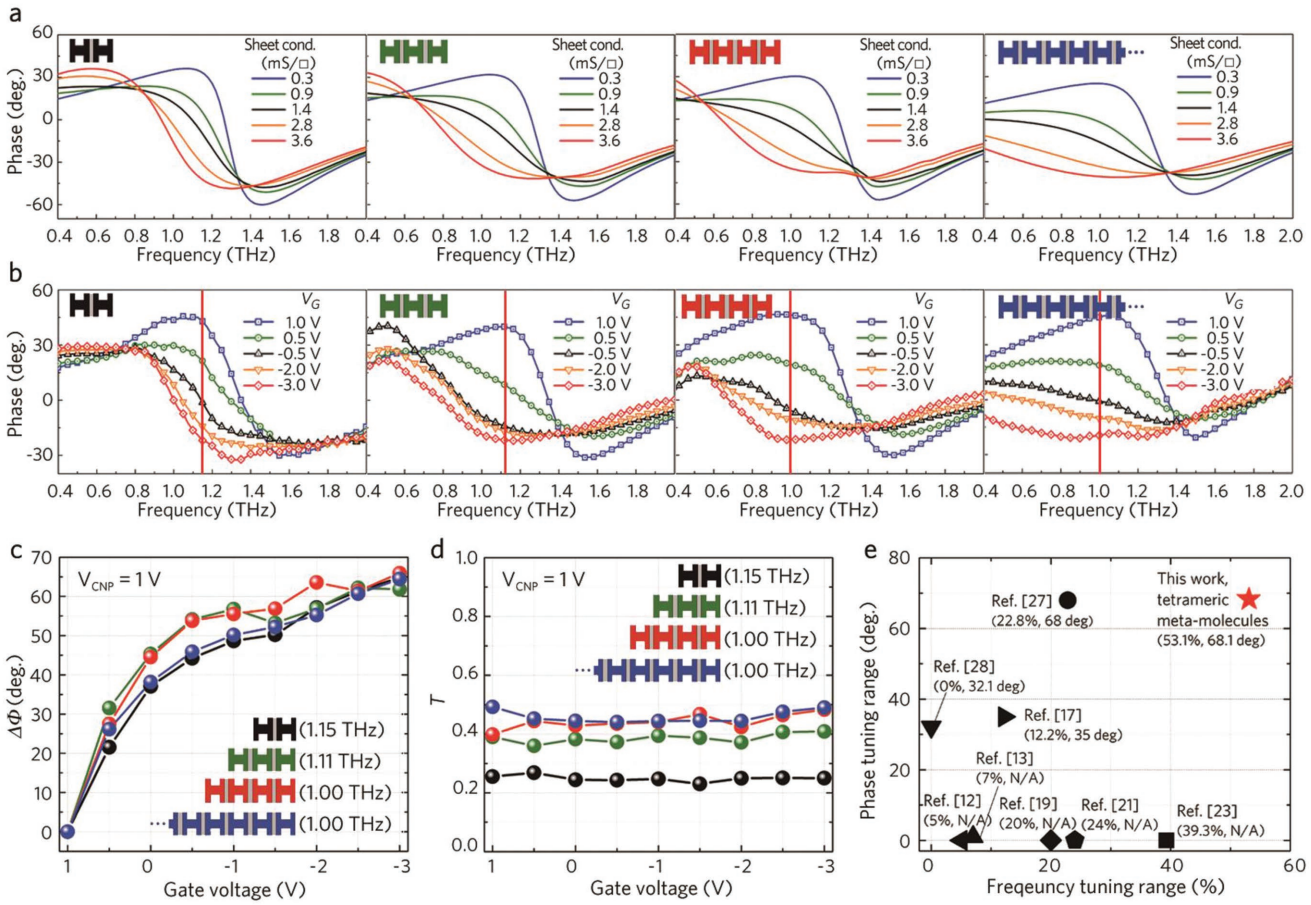

Figure 3. Phase spectra of different-sized metamolecules (simulation and experimental results). a) Simulated and b) experimental phase spectra for dimeric, trimeric, tetrameric, and polymeric metamolecules. c) Phase and d) transmission changes for dimeric, trimeric, tetrameric, and polymeric metamolecules collected at 1.15, 1.11, 1.00, and 1.00 THz, respectively. e) A plot of phase tuning range (in degree) versus frequency tuning range (in %) for the record tetrameric metamolecules in comparison with values from the state-of-the-art tunable THz metamaterials.

negligible within this frequency zone, the change in the slope of the transmission is drastic, and thereby, we can expect the largest $\Delta\phi$ at the zone.

Figure 3 displays the simulated and experimental phase spectra for metamolecules of different sizes at different σ_s values and corresponding V_Gs, respectively. A large change of the phase is clearly observable at different states of molecularizations. Figure 3c plots $\Delta\phi$ as a function of V_G collected at a fixed frequency giving the maximum phase shift for the respective metamolecules, while Figure 3d plots the corresponding variation in T at the fixed frequencies. As V_G varied from 1 V (= V_{CNP}) to −3 V, $\Delta\phi$ increased from 0 up to more than 60 degree for all the molecularization systems. The maximum $\Delta\phi$ value as high as 68.1 degree was obtained at 1.00 THz from the tetrameric metamolecules. As expected, the change in the transmission (ΔT) accompanied with the phase shift was suppressed below 10%; ΔT value for the tetrameric metamolecules was only 7%. Interestingly, the absolute value of the well-retained T increased with the size of the metamolecules. While the absolute T value remained near 25% for the dimeric metamolecules, that for the tetrameric or polymeric metamolecules was pinned around 45%. The enhancement in the absolute T value can be understood from the larger frequency shift between the atomized and molecularized resonances of the larger metamolecules, which eventually leads the overlap of the transmission curves under different V_Gs to occur at higher T. Preserving such a large transmission value with extensive phase control is important for creating a 2π phase shifter by stacking metasurfaces based on well-designed arrays of the proposed metamolecules.

Finally, the tunability of the THz wave for our metamolecularization systems is compared with previous results. Figure 3e displays the tunable range in frequency and phase of the benchmark active metamaterials in the same plot. The red star in the plot is the result obtained from the tetrameric metamolecules, clearly demonstrating the extensive tunability of our THz metamaterials based on the scalable molecularization approach.

In conclusion, we demonstrated an electrically driven device platform for constructing active THz metamaterials. The platform is based on controlling the electrical connection between repeating unit meta-atom structures. By introducing the new concept of molecularization of meta-atoms for THz metamaterials, wider tuning of the resonant frequency as well as their phase, can be achieved from the extendable nature of the approach. The low-voltage operation of the device and the ability to construct the devices on deformable substrates are additional

features of the system. Thus, the scalable approach demonstrated herein is believed to pave the way for advanced metamaterials technologies, such as terahertz sensor, security, and spatial light modulators for single pixel terahertz imaging systems. Moreover, it should be noted that as long as bridging material with good optical conductivity is used,[30] the concept of connecting the meta-atoms and gate tunable bridges is, in principle, applicable to plasmonic metamaterials and optical metasurfaces.

Experimental Section

Array of Meta-Atoms: Metallic structures were patterned on polyimide substrates by using a standard photolithography and lift-off process. Briefly, silicon substrates (iNexus, Inc.) were sonicated using acetone, isopropyl alcohol, and deionized water baths in sequence. Polyimide film was spin-coated onto the silicon substrate (1500 rpm for 40 s), followed by baking the film at 100 °C (3 min) using a hot plate, and at 250 °C (1 h) using a furnace. A 5 µm thick positive photoresist (AZ GXR-650) layer was spin-coated (3500 rpm, 30 s) onto the polyimide film, followed by annealing the substrate at 100 °C on a hot plate. The PR-coated substrate was then exposed to a 350 nm UV-light source through a photomask using a UV aligner. The exposed resist was dissolved in a developer (AZ 300 MIF), and the unexposed resist remained as the sacrificial layer for the lift-off process. After thermally depositing layers of Au/Cr (150/10 nm) onto the substrate, the lift-off process (acetone) yielded metallic metastructures and electrical contacts patterned onto the polyimide film on top of silicon substrates.

Graphene Bridges: Graphene was synthesized by chemical vapor deposition onto a Cu foil. A piece (8 cm × 15 cm) of Cu foil (25 µm, Alfa Aesar) was folded and inserted into a quartz tube. The quartz tube was then inserted into a separate tube furnace. The double-walled configuration was beneficial for reducing the temperature gradient around the Cu foil during the growth. Once the furnace was degassed, the furnace temperature was raised to 1000 °C with H_2 flow (10 sccm) and was maintained at the temperature for the following 30 min. Afterward, CH_4 (15 sccm) and H_2 (10 sccm) were introduced into the tube, while holding the temperature at 1000 °C for another 30 min. Finally, the CH_4 flow was disconnected, and the furnace was rapidly cooled down to room temperature (the H_2 flow was not disconnected during the cooling process). This led to the formation of single-layer graphene grown on both sides of the folded Cu foil. To remove the Cu foil, a solution of poly(methyl methacrylate) (PMMA, MW ≈ 996 000 by GPC, crystalline, Sigma-Aldrich) in chlorobenzene (4.6 g of PMMA was dissolved in 1 L of chlorobenzene, and the mixture was stirred for 12 h before use) was spin-coated onto one side of the unfolded Cu foil deposited with graphene layers on both side. The spinning rate was varied from 500 rpm (7 s) to 4000 rpm (40 s), and to 500 rpm (5 s). Subsequently, the graphene layer formed on one side of the Cu foil that was not coated with PMMA was removed using a reactive ion etching (RIE) system (100 W, 25 s) under O_2 flow (20 sccm). The large Cu foil was cut into small pieces (1 inch by 1 inch) using scissors, and they were floated onto deionized water containing ammonium phosphate (APS) Cu etchant (0.03 M) (7 g of APS (98%, Sigma-Aldrich) was dissolved in 1 L of deionized water, and the mixture was sonicated for 10 min before use). Etching of the Cu foil was done over the next 8–10 h. Once the etching was completely done, the graphene layers floating on the liquid were transferred into a pristine deionized water bath, and were remained floating for 1 h. These floating graphene layers (coated with PMMA) were scooped with the prepatterned substrates with metastructures. The substrates were dried at room temperature for 2 h, and then annealed at 150 °C for the next 40 min. The annealing process helped graphene to adhere onto the substrate. To remove the PMMA layer on graphene, the dried substrates were immersed in acetone for 10 min. This yielded monolayer of graphene on the prepatterned substrates with metastructures. The graphene was patterned by conventional photolithography processes. A positive photoresist (PR501) was applied onto the substrate with graphene layer by spin coating (at 1500 rpm for 5 s, and then at 3000 rpm for the next 30 s), and then the substrate was soft-baked at 100 °C for 1 min. The photoresist layer was exposed to UV through a photomask using a UV aligner, and dipped in a developer (AZ 300 MIF) for 40–50 s. The graphene layer was selectively etched through the photoresist layer using an RIE system (100 W, 25–60 s) under O_2 atmosphere (20 sccm). Finally, the photoresist was removed using acetone.

Ion-Gel Layer: A physically cross-linkable ion-gel solution was applied to the metastructures containing graphene by spin coating (2000 rpm, 1 min) a mixture of polystyrene-poly(methyl methacrylate)-polystyrene (PS-PMMA-PS, 5k–67k–5k, polydispersity index (PDI) = 1.18) and ethyl-methylimidazolium bis(trifluoromethylsulfonyl)imide ([EMIM][TFSI], C-TRI) in ethyl acetate (EA) (wt% PS-PMMA-PS: [EMIM][TFSI]: EA = 1: 9: 22), and annealed at 100 °C for 1 h. Finally, the metamaterials were delaminated from the silicon substrate. Figure S1 (Supporting Information) shows a photograph and an optical microscopy image of the proposed metamaterials on a polyimide film.

Supporting Information

Supporting Information is available from the Wiley Online Library or from the author.

Acknowledgements

H.J. and J.K. contributed equally to this work. This work was supported by Samsung Research Funding Center of Samsung Electronics under Project Number SRFC-MA1601-02.

Conflict of Interest

The authors declare no conflict of interest.

Keywords

graphene, ion gels, metamaterials, molecularization, terahertz

Received: April 30, 2018
Published online: June 14, 2018

[1] W. Withayachumnankul, *IEEE Photonics J.* **2009**, *1*, 99.
[2] T. Kleine-Ostmann, T. Nagatsuma, *J. Infrared, Millimeter, Terahertz Waves* **2011**, *32*, 143.
[3] T. Nagatsuma, G. Ducournau, C. C. Renaud, *Nat. Photonics* **2016**, *10*, 371.
[4] C. Debus, P. H. Bolivar, *Appl. Phys. Lett.* **2007**, *91*, 184102.
[5] H. Tao, L. R. Chieffo, M. A. Brenckle, S. M. Siebert, M. Liu, A. C. Strikwerda, K. Fan, D. L. Kaplan, X. Zhang, R. D. Averitt, F. G. Omenetto, *Adv. Mater.* **2011**, *23*, 3197.
[6] J. Hunt, T. Driscoll, A. Mrozack, G. Lipworth, M. Reynolds, D. Brady, D. R. Smith, *Science* **2013**, *339*, 310.
[7] C. M. Watts, D. Shrekenhamer, J. Montoya, G. Lipworth, J. Hunt, T. Sleasman, S. Krishna, D. R. Smith, W. J. Padilla, *Nat. Photonics* **2014**, *8*, 605.

[8] K. Fan, W. J. Padilla, *Mater. Today* **2015**, *18*, 39.
[9] N.-H. Shen, M. Kafesaki, T. Koschny, L. Zhang, E. N. Economou, C. M. Soukoulis, *Phys. Rev. B* **2009**, *79*, 161102.
[10] S. Sim, H. Jang, N. Koirala, M. Brahlek, J. Moon, J. H. Sung, J. Park, S. Cha, S. Oh, M.-H. Jo, J.-H. Ahn, H. Choi, *Nat. Commun.* **2016**, *6*, 9814.
[11] L. Ju, B. Geng, J. Horng, C. Girit, M. Martin, Z. Hao, H. A. Bechtel, X. Liang, A. Zettl, Y. R. Shen, F. Wang, *Nat. Nanotechnol.* **2011**, *6*, 630.
[12] D. Shrekenhamer, J. Montoya, S. Krishna, W. J. Padilla, *Adv. Opt. Mater.* **2013**, *1*, 905.
[13] M. T. Nouman, H.-W. Kim, J. M. Woo, J. H. Hwang, D. Kim, J.-H. Jang, *Sci. Rep.* **2016**, *6*, 26452.
[14] T. Driscoll, H.-T. Kim, B.-G. Chae, B.-J. Kim, Y.-W. Lee, N. M. Jokerst, S. Palit, D. R. Smith, M. D. Ventra, D. N. Basov, *Science* **2009**, *325*, 1518.
[15] M. Liu, H. Y. Hwang, H. Tao, A. C. Strikwerda, K. Fan, G. R. Keiser, A. J. Sternbach, K. G. West, S. Kittiwatanakul, J. Lu, S. A. Wolf, F. G. Omenetto, X. Zhang, K. A. Nelson, R. D. Averitt, *Nature* **2012**, *487*, 345.
[16] H. Tao, A. C. Strikwerda, K. Fan, W. J. Padilla, X. Zhang, R. D. Averitt, *Phys. Rev. Lett.* **2009**, *103*, 147401.
[17] W. M. Zhu, A. Q. Liu, T. Bourouina, D. P. Tsai, J. H. Teng, X. H. Zhang, G. Q. Lo, D. L. Kwong, N. I. Zheludev, *Nat. Commun.* **2012**, *3*, 1274.
[18] X. Zhao, K. Fan, J. Zhang, G. R. Keiser, G. Duan, R. D. Averitt, X. Zhang, *Microsyst. Nanoeng.* **2016**, *2*, 16025.
[19] H.-T. Chen, J. F. O'hara, A. K. Azad, A. J. Taylor, R. D. Averitt, D. B. Shrekenhamer, W. J. Padilla, *Nat. Photonics* **2008**, *2*, 295.
[20] J. Gu, R. Singh, X. Liu, X. Zhang, Y. Ma, S. Zhang, S. A. Maier, Z. Tian, A. K. Azad, H.-T. Chen, A. J. Taylor, J. Han, W. Zhang, *Nat. Commun.* **2012**, *3*, 1151.
[21] P. Q. Liu, I. J. Luxmoore, S. A. Mikhailov, N. A. Savostianova, F. Valmorra, J. Faist, G. R. Nash, *Nat. Commun.* **2015**, *6*, 8969.
[22] H.-T. Chen, W. J. Padilla, J. M. O. Zide, A. C. Gossard, A. J. Taylor, R. D. Averitt, *Nature* **2006**, *444*, 597.
[23] Y. Zhang, S. Qiao, S. Liang, Z. Wu, Z. Yang, Z. Feng, H. Sun, Y. Zhou, L. Sun, Z. Chen, X. Zou, B. Zhang, J. Hu, S. Li, Q. Chen, L. Li, G. Xu, Y. Zhao, S. Liu, *Nano Lett.* **2015**, *15*, 3501.
[24] M. D. Goldflam, M. K. Liu, B. C. Chapler, H. T. Stinson, A. J. Sternbach, A. S. McLeod, J. D. Zhang, K. Geng, M. Royal, B.-J. Kim, R. D. Averitt, N. M. Jokerst, D. R. Smith, H.-T. Kim, D. N. Basov, *Appl. Phys. Lett.* **2014**, *105*, 041117.
[25] M. M. Jadidi, A. B. Sushkov, R. L. Myers-Ward, A. K. Boyd, K. M. Daniels, D. K. Gaskill, M. S. Fuhrer, H. D. Drew, T. E. Murphy, *Nano Lett.* **2015**, *15*, 7099.
[26] J. H. Cho, J. Lee, Y. Xia, B. Kim, Y. He, M. J. Renn, T. P. Lodge, C. D. Frisbie, *Nat. Mater.* **2008**, *7*, 900.
[27] B. J. Kim, S.-K. Lee, M. S. Kang, J.-H. Ahn, J. H. Cho, *ACS Nano* **2012**, *6*, 8646.
[28] Y. Wu, C. La-o-vorakiat, X. Qiu, J. Liu, P. Deorani, K. Banerjee, J. Son, Y. Chen, E. E. M. Chia, H. Yang, *Adv. Mater.* **2015**, *27*, 1874.
[29] H.-T. Chen, W. J. Padilla, M. J. Cich, A. K. Azad, R. D. Averitt, A. J. Taylor, *Nat. Photonics* **2009**, *3*, 148.
[30] C. McGanhan, K. Appavoo, R. F. Haglund Jr., E. P. Shapera, *J. Vac. Sci. Technol., B* **2013**, *31*, 06FE01.

